Effect of Thermal Annealing on the Kinetics of Rehydroxylation of Eu^{3+}:La$_2$O$_3$ Nanocrystals

Maria Méndez,[†,‡,§] Yolanda Cesteros,[‡] Lluís Francesc Marsal,[§] Alexandre Giguère,[∥] Dominique Drouin,[∥] Pilar Salagre,[‡] Pilar Formentín,[§] Josep Pallarès,[§] Magdalena Aguiló,[†] Francesc Díaz,[†] and Joan Josep Carvajal*[,†]

[†]Física i Cristal·lografia de Materials (FiCMa-FiCNA) and EMaS, Universitat Rovira i Virgili (URV), Campus Sescelades, Marcel·lí Domingo, s/n, E-43007 Tarragona, Spain

[‡]GreenCat-EMaS, Departament Química Física i Inorgànica, Universitat Rovira i Virgili (URV), Campus Sescelades, Marcel·lí Domingo, s/n, E-43007 Tarragona, Spain

[§]Nephos-EMaS, Departament d'Enginyeria Electrònica, Universitat Rovira i Virgili (URV), Campus Sescelades, Avda. Països Catalans, 26, E-43007 Tarragona, Spain

[∥]Department of Electrical and Computer Engineering, Université de Sherbrooke, Sherbrooke, Québec, Canada J1K 2R1

ABSTRACT: Europium-doped lanthanum oxide (5 mol % Eu^{3+}:La$_2$O$_3$) was prepared by calcining europium-doped lanthanum hydroxide (5 mol % Eu^{3+}:La(OH)$_3$) previously synthesized by a simple hydrothermal method. Interestingly, we observed different emission Eu^{3+} signatures depending on the phase of the host (lanthanum oxide or hydroxide) by cathodoluminescence. Taking into account that lanthanum oxide easily rehydroxylates in air, for the first time, we report the use of cathodoluminiscence as a novel characterization technique to follow the lanthanum oxide rehydroxylation reaction versus time according to different annealing procedures. Additionally, differential thermal-thermogravimetric analysis, infrared spectroscopy, and X-ray diffraction techniques were used to identify the phases formed from the Eu^{3+}:La(OH)$_3$ depending on temperature and to study the evolution of La$_2$O$_3$ to La(OH)$_3$ versus time. The results showed that the higher the temperature and the longer the annealing time, the higher the resistance to rehydroxylation of the Eu^{3+}:La$_2$O$_3$ sample.
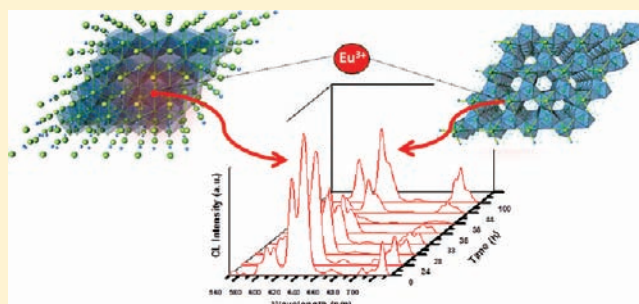
1. INTRODUCTION

Lanthanum oxide is becoming of increasing interest in recent years, due to the wide number of applications of this material together with the possibility of reducing production costs, since in comparison with other rare-earth host materials (Y$_2$O$_3$, Gd$_2$O$_3$, etc.), inorganic compounds containing lanthanum are relatively low-cost host materials.[1] Lanthanum oxide is used in high-potential oxide ceramics,[2] to stabilize the monoclinic phase of zirconia.[3] The hexagonal phase of La$_2$O$_3$, isostructural with γ-Al$_2$O$_3$, has been employed as a component of three-way automotive catalysts,[4−6] as the catalytic active phase for the vapor-phase degradation of 1,4-butanediol,[7] as the catalytic support of metal catalysts for syngas production from dry CO$_2$ re-forming of CH$_4$,[8] and for hydrogen production by steam re-forming and oxidative steam re-forming of ethanol,[9,10] among others. Additionally, this oxide is an important component in some specialized glasses,[11] advanced ceramics,[12−14] and high-temperature superconductors due to its magnetic properties.[15] More recently, La$_2$O$_3$ doped with Eu^{3+} has been used as a phosphor or as a downconverter material of UV light to increase the efficiency of polymers in solar cells.[16−18]

However, lanthanum oxide powders have to be handled carefully because of the activity of the oxide to carbonation and hydroxylation.[19] Lanthanum oxide can react relatively quickly with carbon dioxide/water in the atmosphere to form new stable carbonated and hydroxyl phases through the formation of surface carbonates or hydroxycarbonates. This reaction in air can be completed after 24 h and can drive to mechanical weakness of monolithic pieces.[20−22] Recently, a complete study on the reaction kinetics of the hydroxylation reaction of La$_2$O$_3$ has been published,[23] indicating that the bulk reaction of powders with water vapor proceeds extremely quickly. However, no information about the mechanism involved in this rehydroxylation process has been reported.

The aim of this work is to study the mechanism of rehydroxylation of La$_2$O$_3$ species, in a Eu^{3+}-doped La$_2$O$_3$ sample, after exposition to air at room temperature, and analyze, for the first time, how thermal annealing of the samples affects the kinetics of the rehydroxylation reaction. Cathodo-luminescence (CL) has been used as a novel characterization

technique to follow the lanthanum oxide rehydroxylation versus time according to the different annealing procedures, since Eu³⁺ showed different luminescent spectra (different spectroscopic transitions and different peak ratio intensity) depending on the host containing the active ion (La$_2$O$_3$ or La(OH)$_3$). Additionally, the formation of europium-doped lanthanum oxide from europium-doped lanthanum hydroxide has been also widely characterized.

2. EXPERIMENTAL SECTION

Synthesis of La$_2$O$_3$ Nanocrystals. La$_2$O$_3$ nanocrystals doped with 5 mol % Eu³⁺ were synthesized by a hydrothermal process.[24] A 0.94 g portion of La(NO$_3$)$_3$·6H$_2$O (Fluka, ≥99.9%) and 0.0492 g of Eu(NO$_3$)$_3$·5H$_2$O (Sigma-Aldrich, ≥99.9%) were dissolved in 120 mL of deionized water with stirring for 10 min. Then, 4 g of KOH (Sigma-Aldrich, >85%) was added, leading to a white solution, which was then transferred into a Teflon autoclave and heated to 393 K for 24 h. The resultant white solid product was cleaned with distilled water and ethanol and dried in an air atmosphere at 350 K for 12 h (sample Eu³⁺:La(OH)$_3$). Finally, the dried precipitate was calcined at 1273 K for 2 h to obtain the oxide phase (sample Eu³⁺:La$_2$O$_3$).

Thermal Characterization. Eu³⁺:La(OH)$_3$ was characterized by differential thermal analysis (DTA) and thermogravimetry (TG) to analyze its thermal evolution using a TA Instruments SDT 2960 simultaneous differential techniques instrument. The experiments were carried out in Pt crucibles using calcined Al$_2$O$_3$ as reference material (provided by TA Instruments). Eu³⁺:La(OH)$_3$ was heated at 10 K/min in the 300−1273 K range. Synthetic air was used as the purge gas at a flow rate of 90 cm³/min. The storage rate of data was 0.5 s per data point.

X-ray Diffraction. X-ray diffraction (XRD) measurements were carried out using a Siemens D5000 diffractometer and Ni-filtered Cu Kα radiation (30 mA, 40 kV) with a Braun position sensitive detector (PSD). XRD allowed us to follow the evolution of the crystalline phases from the dried precipitate (Eu³⁺:La(OH)$_3$) by applying a heating rate of 10 K min⁻¹ and the later rehydroxylation reaction versus time of the Eu³⁺:La$_2$O$_3$ nanocrystals just calcined at 1273 K for 2 h. For thermal evolution studies, the 2θ diffraction range was from 10 to 70°, and the measuring time was 10 s per degree in the heating and cooling cycles. Patterns were registered at room temperature and then every 50 K in the interval from 523 to 1073 K under a static air atmosphere, and a delay of 200 s was introduced before each measurement to ensure complete transformation of the sample. At the end of the process, and after the sample was cooled to room temperature, we recorded an additional pattern. For rehydroxylation studies, diffraction patterns were recorded at room temperature in the 2θ range from 25 to 35° at different reaction times up to 40 h.

IR Spectroscopy. The characterization of the evolution of the Eu³⁺:La(OH)$_3$ phase with temperature was also studied by infrared (IR) spectroscopy. The spectra were recorded in the range of 400−3750 cm⁻¹ using a Bruker Equinox-55 Fourier transformed infrared spectrophotometer equipped with a DTGS detector, working in transmission mode. The frequency was set between 50 and 60 Hz, and the current intensity at 0.8 A. The resolution of the measurements was 0.5 cm⁻¹.

Cathodoluminescence. Cathodoluminescence (CL) was recorded at room and low (6 K) temperatures in a field emission scanning electron microscope (LEO Supra 55VP) using a Gatan Mono CL 2 system. The spectra were acquired using a Hamamatsu photomultiplier tube (R2228) at 3−10 keV and using a probe current of 4−7 nA over a scanned area of 10⁴ μm². For this characterization, Eu³⁺:La$_2$O$_3$ and Eu³⁺:La(OH)$_3$ samples were dispersed in an ethanol solution, and several drops of these solutions were deposited on Si substrates, with ethanol allowed to evaporate. By this technique we were able to observe different CL signatures generated by trivalent europium in lanthanum oxide and hydroxide matrices, respectively.

Thermal Annealing. Different thermal annealing treatments were applied to the Eu³⁺:La$_2$O$_3$ nanocrystals prior to their exposure to air atmosphere to investigate the influence of these thermal treatments on

the kinetics of the rehydroxylation reaction. The conventional thermal annealing treatment we used was to heat the sample at 1273 K for 2 h at a heating rate of 10 K min⁻¹. Then, four different rapid thermal annealing procedures were investigated: (i) at 973 K for 1 min (sample A), (ii) at 1073 K for 1 min (sample B), (iii) at 1173 K for 1 min (sample C), and (iv) at 1173 K for 2 min (sample D). After the thermal annealing process we followed the rehydroxylation of the Eu³⁺:La$_2$O$_3$ phase toward the La(OH)$_3$ phase by exposing it to an air atmosphere and recording X-ray diffraction patterns or CL spectra at different times. From the data recorded in these diffraction patterns or CL spectra we developed kinetic curves, defining as the 0 h time the data taken from the patterns or spectra recorded just after the thermal annealing process at room temperature.

3. RESULTS AND DISCUSSION

3.1. Synthesis of La$_2$O$_3$ Nanoparticles from La(OH)$_3$ Precursors. *3.1.1. Thermal Characterization.* With regard to the DTA-TG curve of the Eu³⁺-doped La(OH)$_3$ sample (Figure 1), we identified three different regions, marked as I−III in the
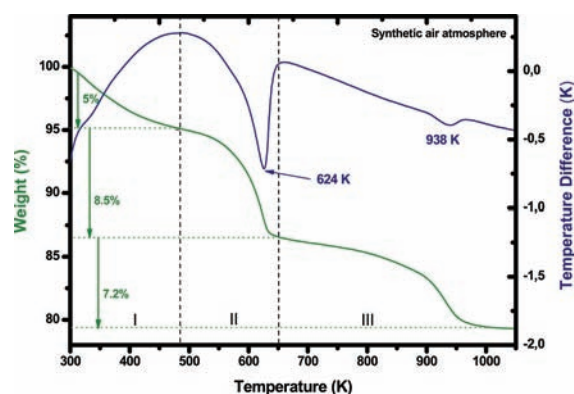

Figure 1. DTA-TG curve of a Eu³⁺:La(OH)$_3$ sample.

figure. Region I, which occurred between 300 and 480 K with a 5% weight loss, can be associated with the evaporation of water. The second and third regions, denoted II and III, respectively, showed endothermic peaks at 624 and 938 K with weight losses of 8.5% and 7.2%, respectively. These two regions can be related to different structural changes of the sample, associated with chemical composition changes. In the literature, these two endothermic peaks have been attributed to the decomposition of La(OH)$_3$ in two steps: first, the formation of lanthanum hydroxide oxide (LaOOH) or different carbonated phases, as intermediate phases, and then at higher temperature the formation of lanthanum oxide (La$_2$O$_3$).[23−26]

3.1.2. Structural Characterization. In order to identify the chemical phase transformations corresponding to regions II and III observed in the DTA-TG curve, the thermal evolution of the dried Eu³⁺-doped La(OH)$_3$ sample was followed by XRD and IR spectroscopy, taking different measurements at different annealing temperatures.

Four different crystalline phases were observed in Figure 2a. The crystalline peaks of the precipitated gel at room temperature were identified as La(OH)$_3$ according to JCPDS file 36-1481.[27] LaOOH phase was not observed at any temperature. In fact, the temperature of the endothermic peak in region II of the DTA thermogram (624 K) (Figure 1) corresponds to an amorphous phase, as observed in the XRD patterns recorded between 623 and 673 K. This amorphous phase evolved with temperature to the carbonated crystalline phase La$_2$O$_2$CO$_3$,[28−30] due to the absorption of atmospheric

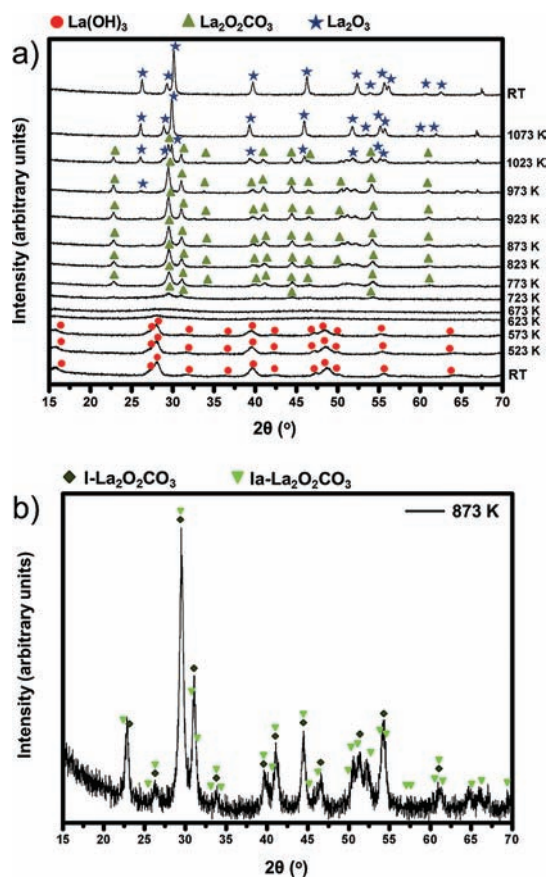**Figure 2.** X-ray diffraction patterns of (a) the transition from Eu^{3+}:$La(OH)_3$ at room temperature to the europium-doped lanthanum oxide phase at 1073 K and (b) the phase obtained at 873 K.

CO_2, since the sample was heated in an air atmosphere. No endothermic or exothermic peaks in the DTA thermogram were observed for the formation of this phase, which was stable at 723 K and from 1023 to 1073 K. Then, this phase disappeared completely to form a new crystalline structure associated with the endothermic peak observed in region III of the thermogram (Figure 1). Turcotte et al. reported the appearance of three different polymorphic forms of $La_2O_2CO_3$ during its decomposition process.[31] According to them, the tetragonal I-$La_2O_2CO_3$ phase (JCPDS file 23-0320),[28] which can be derived from the tetragonal C form of lanthana sesquioxides, formed first. Then, it transformed into an intermediate monoclinic Ia-$La_2O_2CO_3$ phase (JCPDS file 48-1113),[29] and finally, the hexagonal II-$La_2O_2CO_3$ was formed (JCPDS file 37-0804),[30] the structure of which is related to hexagonal La_2O_3 (JCPDS file 74-2430).[32] In our case, we obtained a mixture of tetragonal and monoclinic phases of $La_2O_2CO_3$ (see Figure 2b). We did not detect the hexagonal phase of $La_2O_2CO_3$ but directly determined the formation of La_2O_3. The La_2O_3 phase began to appear at 973 K, coexisting with the $La_2O_2CO_3$ phase, but at 1073 K, La_2O_3 was the only crystalline phase observed in the diffraction pattern. The formation of this phase matched up with the endothermic peak observed at 938 K in the thermogram (Figure 1). After the sample was cooled to room temperature, the same crystalline phase was observed, La_2O_3.

From these results, we can conclude that the calcination of the europium-doped lanthanum hydroxide sample takes place in two steps:
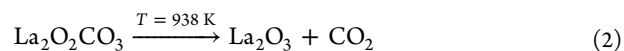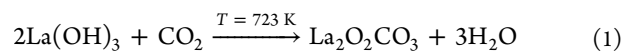
$$2La(OH)_3 + CO_2 \xrightarrow{T = 723\ K} La_2O_2CO_3 + 3H_2O \quad (1)$$

$$La_2O_2CO_3 \xrightarrow{T = 938\ K} La_2O_3 + CO_2 \quad (2)$$

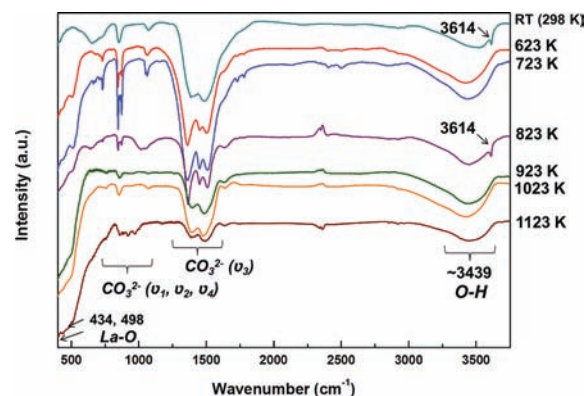Figure 3 shows the thermal evolution of the Eu^{3+}:$La(OH)_3$ phase followed by infrared (IR) spectroscopy. The absorption

Figure 3. Thermal evolution of the infrared spectra of Eu^{3+}:$La(OH)_3$ studied from room temperature to 1123 K.

peaks at 3614 and 3439 cm^{-1} were attributed to the stretching vibration mode of the O−H bond and the bending vibration of H−O−H, respectively. Thus, the peak at 3614 cm^{-1} was indicative of the presence of $La(OH)_3$, whereas the wide band at 3493 cm^{-1} can be associated with water formed during the handling of samples to record the spectra. In the same way, the absorption of carbon dioxide from the atmosphere was confirmed by the appearance of several peaks corresponding to the ν_3 and ν_1, ν_2, and ν_4 modes of the CO_3^{2-} (1636−652 cm^{-1}). This corroborates the presence of $La_2O_2CO_3$, detected by XRD. At higher annealing temperature, the peaks corresponding to $La_2O_2CO_3$ decreased in intensity, whereas the intensity of the broad absorption peaks observed at low wavenumbers (434, 498 cm^{-1}) increased, as expected, due to the formation of the La_2O_3 phase, in agreement with XRD results.

Figure 4 shows the electronic microscopy images of Eu^{3+}:$La(OH)_3$ and Eu^{3+}:La_2O_3 nanocrystals. The precipitated powders are formed by agglomerated nanocrystals of Eu^{3+}:$La(OH)_3$ (Figure 4a), the shapes of which were small nanorods with dimensions around of 30 × 10 nm, as observed by TEM (Figure 4b). After calcination at 1273 K for 2 h, the Eu^{3+}:La_2O_3 nanocrystals showed particles with higher sizes and with less shape definition (Figure 4c) in comparison to those of Eu^{3+}:$La(OH)_3$ (Figure 4b). Therefore, there was a clear effect of the calcination temperature that resulted in a sintering of the nanoparticles, affecting their size and shape.[33]

3.1.3. Spectroscopic Characterization. Figure 5 shows the cathodoluminescence (CL) spectra of (a) Eu^{3+}-doped $La(OH)_3$ and (b) Eu^{3+}-doped La_2O_3 in the 450−750 nm region at room temperature. We ensured that we have only one crystalline phase in the sample, either $La(OH)_3$ or La_2O_3, so that the luminescence peaks appearing in each spectrum could be assigned unequivocally to Eu^{3+} in that crystalline phase. The intensity of the peaks in the region 450−575 nm was increased
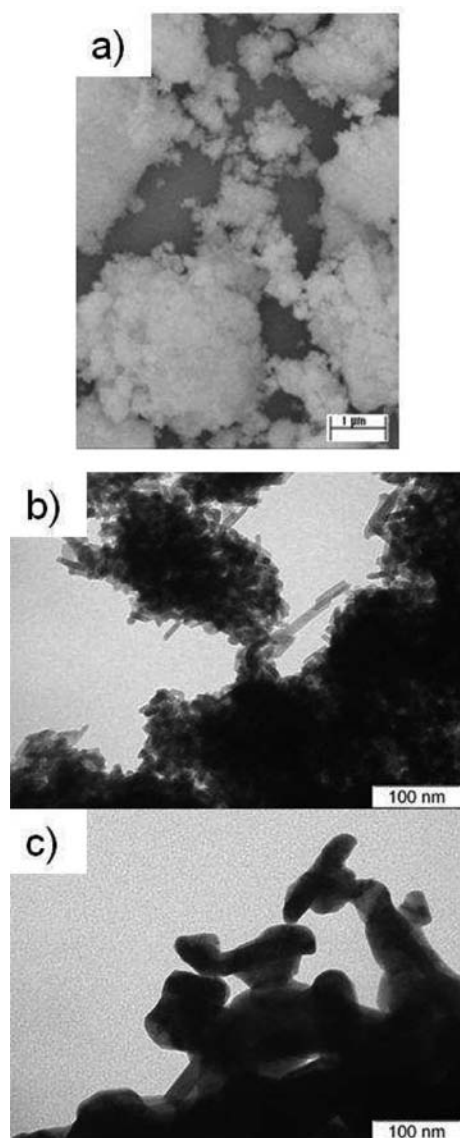
Figure 4. (a) SEM image of $Eu^{3+}:La(OH)_3$ and TEM images of (b) $Eu^{3+}:La(OH)_3$ and (c) $Eu^{3+}:La_2O_3$.

by a factor of $\times 100$ in $Eu^{3+}:La(OH)_3$ and $\times 50$ in $Eu^{3+}:La_2O_3$, since the peaks of this region showed much less intensity than the peaks ranging from 575 to 750 nm.

The different peaks, corresponding to transitions from different ^5D_J ($J = 0-2$) states to $^7F_{J'}$ ($J' = 0-4$) fundamental states, were identified for both structures. The $^5D_0 \rightarrow {}^7F_J$ ($J = 0-4$) and the $^5D_1 \rightarrow {}^7F_J$ ($J = 1, 2$) transitions were observed for Eu^{3+} in $La(OH)_3$. Note in Figure 5a the lower intensity of the bands corresponding to the $^5D_1 \rightarrow {}^7F_J$ ($J = 1, 2$) transitions compared to those corresponding to the $^5D_0 \rightarrow {}^7F_J$ ($J = 0-4$) transitions. For Eu^{3+} in La_2O_3, bands corresponding to the $^5D_0 \rightarrow {}^7F_J$ ($J = 0-4$), $^5D_1 \rightarrow {}^7F_J$ ($J = 1, 2$), and $^5D_2 \rightarrow {}^7F_J$ ($J = 0-3$) transitions could be observed. The $^5D_0 \rightarrow {}^7F_J$ ($J = 0-4$) transitions showed higher intensity than the $^5D_1 \rightarrow {}^7F_J$ ($J = 1, 2$) transitions, while the $^5D_2 \rightarrow {}^7F_J$ ($J = 0-3$) transitions exhibited the lowest intensity (Figure 5b). The most intense emission peak was centered at 615 nm in the $Eu^{3+}:La(OH)_3$ spectrum and at 626 nm in the $Eu^{3+}:La_2O_3$ spectrum, corresponding to the $^5D_0 \rightarrow {}^7F_2$ transition in both cases. Since this peak was the most intense for both structures, this

indicates that Eu^{3+} was located in a structural site without an inversion center,[34] such as the crystallographic site occupied by La^{3+} in these structures, S_3 in $La(OH)_3$ and C_{3v} in La_2O_3.[34,35] The observation of the $^5D_0 \rightarrow {}^7F_0$ transition in these two structures is also an indication that Eu^{3+} was located in these crystallographic sites, since this transition should be completely forbidden at first order but might be partially allowed in the presence of a linear crystal field term.

The $2J + 1$ degeneracy of the free ion may be broken by the crystal field at its location. The levels with $J = 0$ are nondegenerate; therefore, if only one structural position for Eu^{3+} in the crystalline structure exists, the $^5D_0 \rightarrow {}^7F_0$ transition should have only one peak, while the $^5D_0 \rightarrow {}^7F_1$ transition should exhibit three peaks and the $^5D_0 \rightarrow {}^7F_2$ transition should show five peaks. In the spectra presented in Figure 5a,b, the $^5D_0 \rightarrow {}^7F_0$ transition seems to show only one peak for both structures, while the $^5D_0 \rightarrow {}^7F_1$ and the $^5D_0 \rightarrow {}^7F_2$ transitions show more than one peak in the case of $Eu^{3+}:La_2O_3$ and several shoulders in the case of $Eu^{3+}:La(OH)_3$. To verify this aspect, we recorded CL spectra of the $Eu^{3+}:La(OH)_3$ and $Eu^{3+}:La_2O_3$ samples at 6 K (see Figure 5c,d, respectively). Both spectra show only one peak for the $^5D_0 \rightarrow {}^7F_0$ transition, confirming that only one structural position for Eu^{3+} exists in the crystalline structure of these two compounds. However, the fine structure of the $^5D_0 \rightarrow {}^7F_1$ and the $^5D_0 \rightarrow {}^7F_2$ transitions was still not well resolved, since the system does not allow a recording resolution for the spectra of higher than 0.5 nm. This effect is more pronounced for the $Eu^{3+}:La(OH)_3$ sample than for the $Eu^{3+}:La_2O_3$ sample.

The intensity of the electric dipolar $^5D_0 \rightarrow {}^7F_2$ transition (hypersensitive) is very sensitive to the crystal field generated by the ligands. Although the $^5D_0 \rightarrow {}^7F_1$ transition is a magnetic dipole transition, and its intensity is independent of the local environment of Eu^{3+}, it can be taken as a reference for different materials. Furthermore, the ratio between the intensities of the $^5D_0 \rightarrow {}^7F_2$ and the $^5D_0 \rightarrow {}^7F_1$ transitions, known as the I_2 ratio or asymmetry ratio, provides an approximation of the distortion degree of the coordination polyhedron of the Eu^{3+} ion in a particular matrix. The intensity ratios I_2 were 1.3 and 7.2 for $Eu^{3+}:La(OH)_3$ and $Eu^{3+}:La_2O_3$, respectively. On one hand, in comparison with other ratios reported in the literature,[34,36,37] the value obtained for the La_2O_3 matrix is within the maximum values reported. A high value of this ratio indicates that the electric dipole interaction is enhanced, associated with a stronger crystal field in the short range, which can be related to an increase of the covalence of the structure or to a distortion of the bonds surrounding the active ion. On the other hand, the value obtained for the $La(OH)_3$ matrix is within the minimum values. Thus, by comparing these two structures, we should expect that, although in both cases Eu^{3+} was located in a low-symmetry site, the oxygen atoms surrounding Eu^{3+} formed a more regular polyhedron in $La(OH)_3$ than in La_2O_3. In fact, the coordination polyhedron of La^{3+} in $La(OH)_3$ is formed by nine oxygen atoms, three of which are located at a distance of 2.551 Å, and six additional oxygen atoms at a distance of 2.588 Å.[38] In contrast, for La_2O_3, La^{3+} is surrounded by seven oxygen atoms located at distances ranging from 2.356 to 2.743 Å. The distortion of the polyhedron is defined as $\Delta d = (1/t)\sum_{n=1-t}\{[d(La-O)_n - \langle d(La-O)\rangle]/\langle d(La-O)\rangle\}^2$, where t is the number of surrounding oxygen atoms around La and $\langle d(La-O)\rangle$ is the mean La–O distance. Thus, the polyhedron distortions were 4.6×10^{-5} and 5.2×10^{-3} for $La(OH)_3$ and La_2O_3 structures, respectively. It is easy to note that the value of
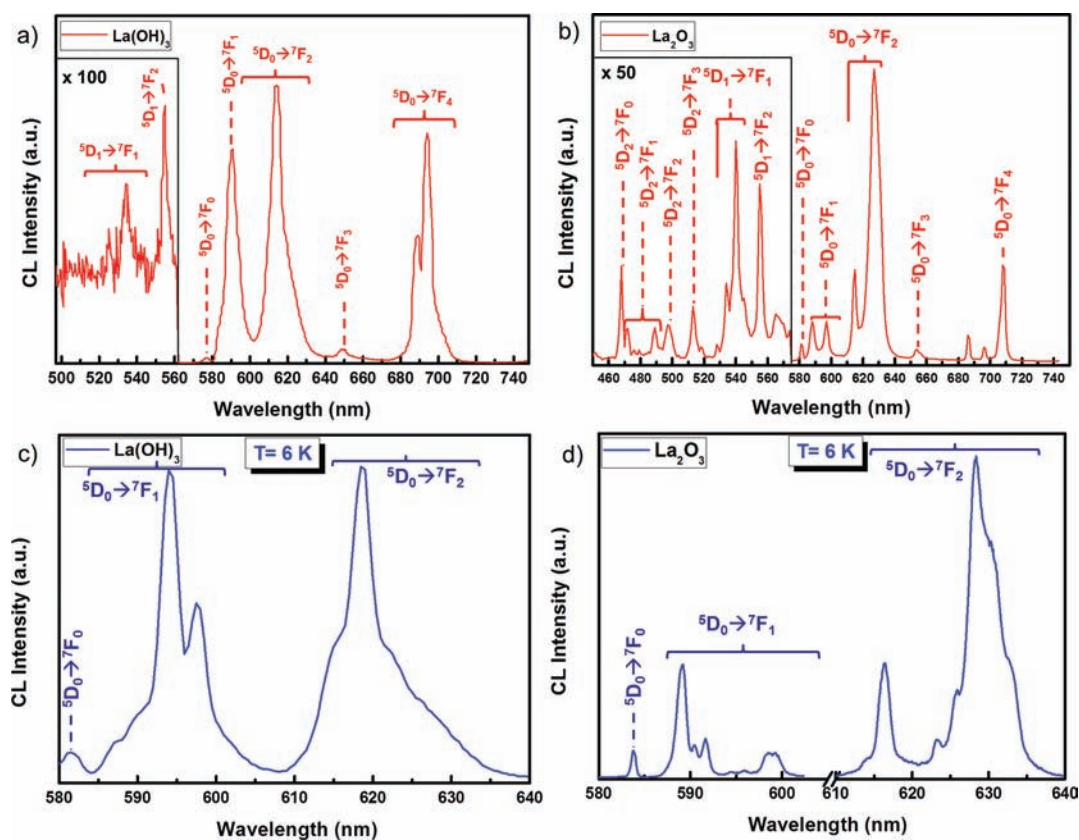
Figure 5. Cathodoluminescence spectra recorded at room temperature for (a) Eu^{3+}:$La(OH)_3$ and (b) Eu^{3+}:La_2O_3 and at low temperature for (c) Eu^{3+}:$La(OH)_3$ and (d) Eu^{3+}:La_2O_3.

La_2O_3 was 2 orders of magnitude higher than the value obtained for the $La(OH)_3$ structure.[39]

3.2. Rehydroxylation of the La₂O₃ Nanocrystals.

3.2.1. Structural Characterization.

We monitored the evolution of the rehydroxylation reaction of Eu^{3+}:La_2O_3 nanoparticles with time by XRD. Rehydroxylation is due to the absorption of water moisture from the atmosphere, which has been reported to be responsible for the fast transformation of La_2O_3 into $La(OH)_3$.[23] To study this transformation, we previously calcined Eu^{3+}:$La(OH)_3$ at 1273 K for 2 h to guarantee only the presence of the oxide phase. Figure 6 shows the dynamics of the rehydroxylation reaction of Eu^{3+}:La_2O_3 monitored by XRD. The range of measurement has been restricted in this case from 25 to 35°. We marked with a star the three most intense peaks of La_2O_3 to make the observation of the chemical conversion easier for the reader. These peaks correspond to the (100), (002), and (101) reflections.[32] Regarding Figure 6, we could note that the La_2O_3 phase was stable up to 30 h. The evolution of the three diffraction peaks on which we focused our attention to follow the chemical conversion is marked with a blue line in Figure 6. We also observed that the La_2O_3 phase started to disappear at the same time that the $La(OH)_3$ phase began to appear at about 25 h. Thus, in the range between 25 and 30 h, both phases were present.

Another interesting point is that during rehydroxylation no intermediate phases were observed, neither crystalline nor amorphous, and the conversion evolved directly from the oxide to the hydroxide phase. We evaluated the kinetic curve of the rehydroxylation reaction by relating the intensity of the (101) diffraction peak of $La(OH)_3$ to its concentration in the sample.

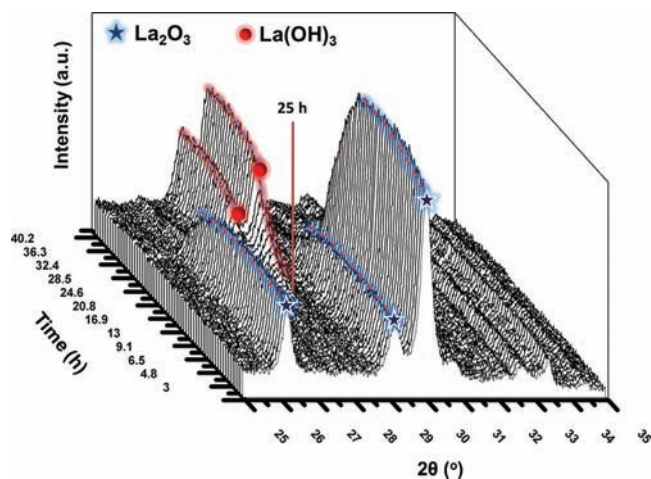**Figure 6.** Evolution of the X-ray powder diffraction pattern of Eu^{3+}:La_2O_3 versus time after exposure to air atmosphere at room temperature.

The result is presented in Figure 7. More than 22 h was needed to convert 50% of La_2O_3 to $La(OH)_3$, and after 35 h, La_2O_3 was completely rehydroxylated.

3.2.2. Spectroscopic Characterization after Different Annealing Procedures.

CL measurements confirmed the kinetic transformation. Table 1 gives the wavelengths of the different emission bands observed for electronic transitions at room temperature in Eu^{3+}:$La(OH)_3$ and Eu^{3+}:La_2O_3 (see Figure 5a,b). After following the evolution of the sample annealed at 1273 K for 2 h by applying a heating rate of 10 K

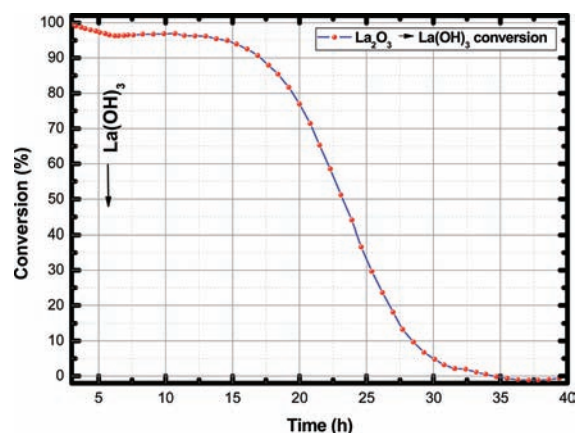**Figure 7.** Kinetic curve of the rehydroxylation process after calcining $Eu^{3+}:La(OH)_3$ at 1273 K for 2 h at a heating rate of 10 K min^{-1} and evaluating by XRD.

Table 1. Wavelength Values of the Cathodoluminescence Peaks of $Eu^{3+}:La(OH)_3$ and $Eu^{3+}:La_2O_3$

transition	La(OH)$_3$ peak position (nm)	La$_2$O$_3$ peak position (nm)
$^5D_2 \rightarrow {}^7F_0$		468
$^5D_2 \rightarrow {}^7F_1$		472, 475, 479, 489
$^5D_2 \rightarrow {}^7F_2$		497
$^5D_2 \rightarrow {}^7F_3$		512
$^5D_1 \rightarrow {}^7F_1$	524, 534	533, 540
$^5D_1 \rightarrow {}^7F_2$	555	554
$^5D_0 \rightarrow {}^7F_0$	577	581
$^5D_0 \rightarrow {}^7F_1$	591	588, 596
$^5D_0 \rightarrow {}^7F_2$	613	614, 626
$^5D_0 \rightarrow {}^7F_3$	648	653
$^5D_0 \rightarrow {}^7F_4$	688, 694	708

min^{-1} and later studying its corresponding kinetic curve (Figure 7), we analyzed what happened if we applied rapid thermal annealing conditions: 973 K for 1 min (sample A), 1073 K for 1 min (sample B), 1173 K for 1 min (sample C), and 1173 K for 2 min (sample D).

Just after samples A−D were annealed at different experimental conditions, the CL spectra showed the typical bands of Eu^{3+} in La_2O_3, as expected. However, we observed that the relative intensity between the two peaks corresponding to the $^5D_0 \rightarrow {}^7F_2$ transition, located at 613 and 626 nm, called the intensity ratio I_1, changed significantly with time, with a reduction of the intensity of the peak located at 626 nm. At longer time, the rehydroxylation progressed and I_1 further decreased. Finally, the 613 nm band, corresponding to the $^5D_0 \rightarrow {}^7F_2$ transition in La(OH)$_3$, dominated the spectra. At the same time, the emission band located at 707 nm, corresponding to the $^5D_0 \rightarrow {}^7F_4$ transition in $Eu^{3+}:La_2O_3$, lost intensity, whereas the emission band located at 695 nm, corresponding to the same transition than the band located at 707 nm, was more and more intense. Parts a−d of Figure 8 show the CL spectra of samples A−D. The cathodoluminescence spectra were recorded at different times after the annealing process (0, 24, 28, 33, 35, 38, 44, and 100 h). From these spectra, we observed that the La(OH)$_3$ phase appeared after 24 h of annealing, but the sample was not completely transformed to La_2O_3 until 35−38 h, since the cathodoluminescence spectra of the sample no longer changed. However, the kinetics of the rehydroxylation

reactions progressed differently, depending on the annealing procedure (time and temperature).

The kinetic curves obtained from the cathodoluminescence spectra of samples A−D are also shown in order to observe the differences with respect to the annealing procedure in more detail. Figure 9 shows the kinetic curves depending on temperature (Figure 9a, 973, 1073, and 1173 K) and depending on time (Figure 9b, 1 and 2 min). Time 0 h corresponds to the measurements taken just after the annealing procedure. After that, the samples were exposed to air at room temperature. We observed that when the annealing temperature was higher, the rehydroxylation process evolved more slowly (Figure 9a). On one hand, sample A, which was annealed at 973 K, showed 100% of conversion after 38 h of annealing, whereas the samples B and C (annealed at 1073 and 1173 K, respectively) showed about 88% and 82% of conversion, respectively. On the other hand, the shape of the curve of the rehydroxylation was also significant. For instance, we observed that by increasing the temperature from 973 to 1073 K, after 30 h of the annealing process, sample A lost 75% of the oxide to hydroxide phase while sample B just lost 12% of the oxide phase. Figure 9b shows the kinetic curve after annealing the sample at 1173 K for 1 min (sample C) and 2 min (sample D). After 40 h, only ∼50% of sample D was converted to $Eu^{3+}:La(OH)_3$, while almost 85% of sample C was already converted to $Eu^{3+}:La(OH)_3$. Thus, at the same annealing temperature, the rehydroxylation process evolved more slowly when we increased the time of annealing. However, the full conversion of the material was achieved at the same time, indicating that the reaction evolved more slowly at the beginning for sample D but more quickly at the end. These results could be compared with the kinetic curves depending on the temperature because the most significant difference between samples A−C and samples C and D was the resistance time of the $Eu^{3+}:La_2O_3$ to be rehydroxylated. Thus, everything indicated that after a certain degree of conversion achieved, the reaction evolved more quickly. When comparing these results with those obtained previously by conventional annealing techniques (1273 K for 2 h), we could see that rapid thermal annealing increased the stability of La_2O_3, which constituted a benefit of manipulating this compound under a noncontrolled atmosphere.

4. CONCLUSIONS

We successfully synthesized 5 mol % $Eu^{3+}:La_2O_3$ by a simple and clean hydrothermal method followed by calcination. During the transformation of $Eu^{3+}:La(OH)_3$ to $Eu^{3+}:La_2O_3$, an intermediate and amorphous phase, identified as $La_2O_2CO_3$, was detected by XRD. This phase had two components: tetragonal (I-$La_2O_2CO_3$) and monoclinic (Ia-$La_2O_2CO_3$). The sample $Eu^{3+}:La_2O_3$ was completely rehydroxylated after 40 h of exposure to moisture.

We characterized carefully the emission spectroscopy of both samples, 5 mol % $Eu^{3+}:La_2O_3$ and 5 mol % $Eu^{3+}:La(OH)_3$, by cathodoluminiscence. Interestingly, by resolving the emission peaks of both phases, we were able to study the transition from one phase to the other and the effect of the annealing conditions on the kinetics of the rehydroxylation reaction. The results showed that the annealing process used in the calcination of the samples plays a major role in the kinetics of the rehydroxylation reaction. We observed that the higher the temperature and the longer the annealing time, the more the resistance to rehydroxylation of the $Eu^{3+}:La_2O_3$ formed.
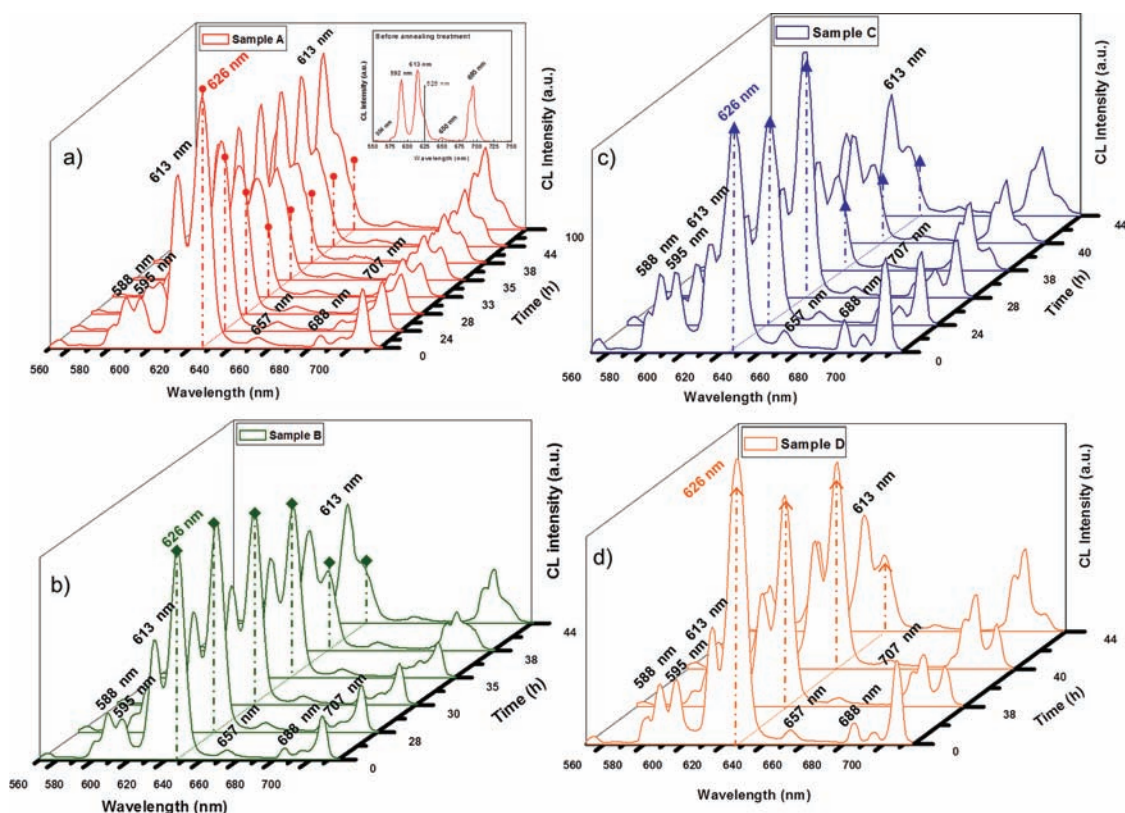
Figure 8. Cathodoluminescence spectra of (a) sample A annealed at 973 K for 1 min (the inset figure shows the cathodoluminescence spectra of the precipitated gel Eu^{3+}:$La(OH)_3$), (b) sample B annealed at 1073 K for 1 min, (c) sample C annealed at 1173 K for 1 min, and (d) sample D annealed at 1173 K for 2 min.
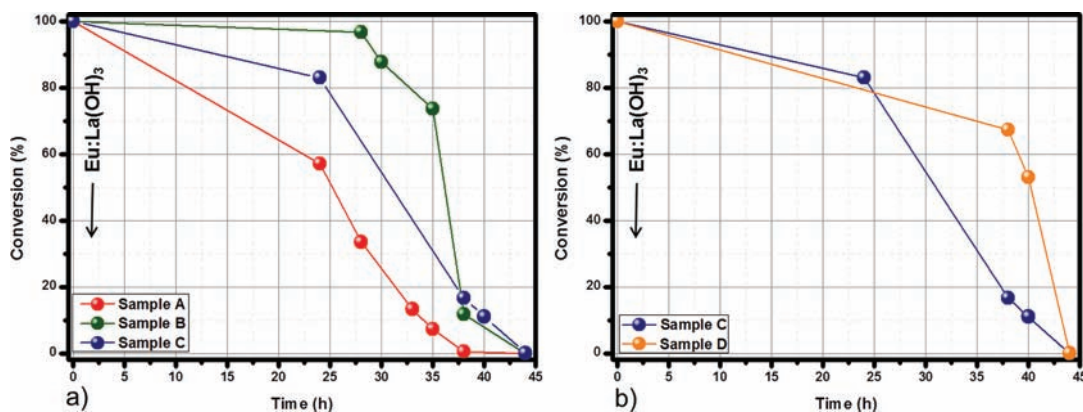

Figure 9. Kinetic curves of the rehydroxylation process depending on (a) temperature and (b) time.

However, when a lower heating rate was also used (10 K min^{-1}), the Eu^{3+}:La_2O_3 nanocrystals converted more quickly toward Eu^{3+}:$La(OH)_3$.

These results give new data on the stability of Eu^{3+}:La_2O_3 exposed to the atmosphere and show how, by applying rapid thermal annealing processes at high temperatures and for long periods of time, we can increase the stability of this compound and slow down the kinetics of the rehydroxylation reaction. These results are important, especially for those applications that require a manipulation of these compounds in non-controlled environments, since we can minimize the rehydroxylated portion of Eu^{3+}:La_2O_3.

■ **AUTHOR INFORMATION**

Corresponding Author
*E-mail: joanjosep.carvajal@urv.cat.

Notes
The authors declare no competing financial interest.

by the Research Center on Engineering of Materials and Systems (EMaS).

■ REFERENCES

(1) Liu, J.; Fei, X.; Yu, X.; Tao, Z; Yang, L; Yang, S. *J. Non-Cryst. Solids* **2007**, *353*, 4697.

(2) Antunes, A. C.; Antunes, S. R. M.; Pianaro, S. A.; Longo, E.; Leite, E. R.; Varela, J. A. *J. Mater. Sci. Mater. El.* **2001**, *12*, 69.

(3) Mercera, P. D. L.; Vanommen, J. G.; Doesburg, E. B. M.; Burggraaf, A. J.; Ross, J. R. H. *Appl. Catal.* **1991**, *71*, 363.

(4) George, A. M.; Mishra, N. C.; Jayadeva, N. C. *J. Mater. Sci.* **1992**, *11*, 404.

(5) Trovarelli, A. *Catal. Rev. Sci. Eng.* **1996**, *38*, 439.

(6) Tanabe, T.; Nagai, Y.; Dohmae, K.; Takagi, N.; Takahashi., N.; Matsumoto, S.; Shinjoh., H. *Appl. Catal. B: Environ.* **2011**, *105*, 41.

(7) Sato, S.; Takahashi, R.; Kobune, M.; Inoue, H.; Izawa, Y.; Ohno, H.; Takahashi, K. *Appl. Catal. A: Gen.* **2009**, *356*, 64.

(8) Sutthiumporn, K.; Kawi, S. *Int. J. Hydrogen Energy* **2011**, *36*, 14435.

(9) de Lima, S. M.; da Silva, A. M.; da Costa, L. O. O.; Assaf, J. M.; Jacobs, G.; Davis, B. H.; Mattos, L. V.; Noronha, F. B. *Appl. Catal. A: Gen.* **2010**, *377*, 181.

(10) Chen, H.; Yu, H.; Peng, F.; Wang, H.; Yang, J.; Pan, M. *J. Catal.* **2010**, *269*, 281.

(11) Hussein, G. A. M. *J. Anal. Appl. Pyrol.* **1996**, *37*, 111.

(12) Huang, Z. K.; Liu, S. Y.; Rosenflanz, A.; Chen, I. W. *J. Am. Ceram. Soc.* **1996**, *79*, 2081.

(13) Shuba, R.; Chen, I. W. *J. Am. Ceram. Soc.* **2006**, *89*, 2860.

(14) Yang, Z.; Wang, H.; Min, X.; Wang, W.; Fu, Z.; Lee, S. W.; Niihara, K. *J. Eur. Ceram. Soc.* **2012**, *32*, 931.

(15) Schulte, B.; Maul, M.; Becker, W.; Schlosser, E. G.; Haussler, P.; Adrain, H. *Appl. Phys. Lett.* **1991**, *59*, 869.

(16) Park, J. K.; Park, S. M.; Kim, C. H.; Park, H. D.; Choi, S. Y. *J. Mater. Sci. Lett.* **2001**, *20*, 2231.

(17) Lui, H.; Wang, L.; Chen, S.; Zuo, B. *J. Lumin.* **2007**, *126*, 459.

(18) Méndez, M.; Cesteros, Y.; Marsal, L. F.; Martínez-Ferrero, E.; Salagre, P.; Formentín, P.; Pallarès, J.; Aguiló, M.; Díaz, F.; Carvajal, J. J. *Opt. Mat.* **2011**, *33*, 1120.

(19) Bernal, S.; Botana, F. J.; Garcia, R.; Rodríguez-Izquierdo, J. M. *React. Solids* **1987**, *4*, 23.

(20) Klingenberg, B.; Vannice, M. A. *Chem. Mater.* **1996**, *8*, 2755.

(21) Siegmann, H. C.; Schlapbach, J.; Brundle, C. R. *Phys. Rev. Lett.* **1978**, *40*, 972.

(22) Fleisch, T. H.; Hicks, R. F.; Bell, A. T. *J. Catal.* **1984**, *87*, 398.

(23) Fleming, P.; Farrell, R. A.; Holmes, J. D.; Morris, M. A. *J. Am. Ceram. Soc.* **2010**, *93*, 1187.

(24) Ino, E.; Shimizu, K.; Yamate, T. *Zairyo* **1976**, *25*, 1165.

(25) Rosynek, M. P.; Magnuson, D. T. *J. Catal.* **1977**, *46*, 402.

(26) Neumann, A.; Walter, D. *Tagungsband zur Wöhler-Tagung* **2004**, 4.

(27) Beall, G. W.; Milligan, M. O.; Wolcott, H. A. *J. Inorg. Nucl. Chem.* **1977**, *39*, 65.

(28) Powder Diffraction File Database PDF-2, International Center for Diffraction Data, ICDD, 2010, File 23-0320.

(29) Powder Diffraction File Database PDF-2, International Center for Diffraction Data, ICDD, 2010, File 48-1113.

(30) Powder Diffraction File Database PDF-2, International Center for Diffraction Data, ICDD 2010, File 37-0804.

(31) Turcotte, R. P.; Sawyer, J. O.; Eyring, L. *Inorg. Chem.* **1969**, *8*, 238.

(32) Mueller-Buschbaum, H.; von Schnering, H. G. *Z. Anorg. Allg. Chem.* **1965**, *340*, 232.

(33) Galceran, M.; Pujol, M. C.; Carvajal, J. J.; Mateos, X.; Zaldo, C.; Aguiló, M.; Diaz, F. *J. Lumin.* **2010**, *130*, 1437.

(34) Ninjbadgar, T.; Garnweitner, G.; Börger, A.; Goldenberg, L. M.; Sakhno, O. V. *J. Adv. Funct. Mater.* **2009**, *19*, 1819.

(35) Hahn, T. *International Tables for Crystallography*; The International Union of Crystallography; D. Reidel: Dordrecht, The Netherlands, 1987; Vol. A.

(36) Liu, G.; Chen, X. In *Handbook on the Physics and Chemistry of Rare Earth*; Gschneidner, K. A., Jr., Eyring, L., Eds.; Elsevier North Holland: Amsterdam, 2007; Chapter 37, p 99.

(37) Liu, H. Q.; Wang, L. L.; Huang, W.; Peng, Z. W. *Mater. Lett.* **2007**, *61*, 1968.

(38) Milligan, W. O.; Mullica, D. F.; Oliver, J. D. *J. Appl. Crystallogr.* **1979**, *12*, 411.

(39) Koehler, W. C.; Wollan, E. O. *Acta Crystallogr.* **1953**, *6*, 741.